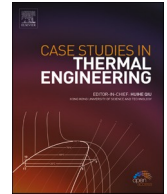




ELSEVIER

Contents lists available at ScienceDirect

Case Studies in Thermal Engineering

journal homepage: www.elsevier.com/locate/csite

Numerical investigation of heat transfer and water infiltration characteristics within two-dimensional granular packed beds

Sauce Aksornkitti^{a,*}, Phadungsak Rattanadecho^{a,**}, Teerapot Wessapan^{b,***}

^a Center of Excellence in Electromagnetic Energy Utilization in Engineering (CEEE) Department of Mechanical Engineering, Faculty of Engineering, Thammasat University (Rangsit Campus), 99 Moo 18, Klong Luang, Pathum Thani, 12120, Thailand

^b Department of Mechanical Engineering, Faculty of Engineering, Rajamangala University of Technology Thanyaburi, 39 Moo 1, Klong 6, Klong Luang, Pathum Thani, 12110, Thailand

ARTICLE INFO

Keywords:

Infiltration
Temperature
Water saturation
Porous packed bed
Heat transfer

ABSTRACT

This study used numerical analysis to determine the transport phenomena of hot water infiltration in a two-dimensional granular packed bed. The present study aims to investigate the parameter that affects the water saturation and temperature distribution in the two-dimensional porous packed bed. For this purpose, the problem was solved numerically using two-dimensional unsaturated flow and heat transfer models of hot water infiltration. Novel studies on the simultaneous heat and moisture transfer during hot water infiltration in partially saturated porous materials were investigated. The study illustrated the characteristics of heat and moisture transfer during the water infiltration process in various testing conditions. The results of the numerical model were validated with the results from previous research. It was found that the water flux supplied, and particle size have significant effects on the distribution of water saturation and temperature in the packed bed. The water saturation and heating area of the fine particles tended to expand in the lateral direction faster than the downward direction. The increase in supplied water flux resulted in a deeper and larger zone of water saturation and heating area. Furthermore, the heating area was found to be expanding slower than the water saturation front in all conditions.

1. Introduction

In recent decades, a physical understanding of the infiltration process in the porous material is an important research frontier, which is crucial for implementing novel applications in many directions. Fundamental understanding of infiltration process in porous material can be used for numerous creative and innovative applications in several fields of engineering and medicine, including needle-free drug delivery system, percutaneous infiltration, noninvasive ultrasonic facial rejuvenation system, subsurface flow, soil science, crop irrigation [1–5]. In many aspects, biological tissue can also be compared with heterogeneous porous media. Biological cells and tissues are heterogeneous in structure with cellular diversity, where the majority of the water is located in the spaces. This pore space can be occupied by fluids. The understanding of infiltration effects in porous media is also an essential step in developing

* Corresponding author.

** Corresponding author.

*** Corresponding author.

E-mail addresses: sauce2528@gmail.com (S. Aksornkitti), ratphadu@engr.tu.ac.th (P. Rattanadecho), teerapot_w@rmutt.ac.th (T. Wessapan).

<https://doi.org/10.1016/j.csite.2021.101417>

Received 28 May 2021; Received in revised form 11 August 2021; Accepted 2 September 2021

Available online 4 September 2021

2214-157X/© 2021 Published by Elsevier Ltd. This is an open access article under the CC BY-NC-ND license

(<http://creativecommons.org/licenses/by-nc-nd/4.0/>).

advanced technology within the biomedical field (e.g., tissue fluid infiltration, needle-free injection technology, and submucosal tumor infiltration). The water infiltration process in the porous material is linked to various gravity-induced mass-transport processes. Water infiltration is influenced by various factors. The intrinsic factors influencing the water infiltration process are the hydraulic parameters, transmissivity, and permeability of the porous medium. The extrinsic factors are mainly related to external parameters, such as surrounding temperature and ambient conditions.

Several different types of factors that can influence the infiltration characteristics of unsaturated porous media have been extensively investigated and highlighted by studies in this field [6–16]. Hammecker et al. [6] carried out the experiment on measurements with various methods and found that the soil-water movement was controlled by the trapped air remained at the wetting fronts. Gvirtzman et al. [7] carried out the experiment on tracking water movement in the unsaturated stratified media. The results indicated that the developed hydrostatic pressure within saturated porous layers, increases the water front propagation distance. Ma et al. [8] presented an infiltration experiment of soil to validate the proposed updated infiltration model against the standard Green-Ampt model. The fitting of experimental data showed that the proposed model served as an efficient tool for estimation of water infiltration into layered soils, and the employed saturation parameter represented the influence of air trapping on water movement. Ayu et al. [9] carried out to measure the infiltration rate on various types of soil in dryland areas using the double-ring infiltrometer. The data analysis revealed that soil properties affecting infiltration rate in the research locations were sand and clay percentages, soil moisture content, bulk density, particle density, soil organic matter, and soil porosity. Langston and Kennedy [10] developed a numerical model to test spectroscopic parameters of NaCl beads at different sizes. The excellent literature reviews summarized the water flow in porous material with saturation overshoot have been provided by Xiong [11]. Representative works, for related numerical problems of unsaturated flow under infiltration conditions for different applications, include Henry and Smith [12], Romano et al. [13], Corradini et al. [14], Gomez et al. [15], Sayah et al. [16].

However, a fundamental understanding of heat transfer behavior during water infiltration into unsaturated porous media is important in a variety of biomedical science, soil science, and engineering, such as thermo-responsive drug delivery systems, soil temperature regulation, and geo-heat recovery. Thus, the heat transfer investigation in the infiltration process was also considered. Several factors that can influence the heat transfer during the infiltration process in different media have also been extensively studied. Bandai et al. [17] experimented to investigate the influence of particle size on dispersion and heat transfer in porous media. The study showed that the thermal dispersion coefficient was influenced by particle size. A few numerical investigations have also been carried out by some researchers. D. Gobin et al. [18] developed a mathematical model for the solidification and infiltration of liquid metal in porous structures. The developed model was used to determining the effect of the operating parameters on the depth and time of the solidification in simple geometry. Our research group has also been studying for a coupled heat transfer with water infiltration in the porous medium [19,20]. Suttisong and Rattanadecho [19] conducted an experiment to determine the water flow and heat transport in a vertical packed column. The findings showed that larger particles result in increased infiltration rate and heat transfer. Rattanadecho et al. [20] carried out a 1D mathematical model of the infiltration and heat transfer in a vertical packed column. The calculated temperature distribution and water saturation were compared to experiments. It was discovered that a higher water flux supplied corresponded to the temperature increase and water saturation. There were many attempts associated with convection flow within porous enclosures using the recently proposed Incompressible Smoothed Particle Hydrodynamics (ISPH) method. Aly et al. [21,22] carried out research on convective flows of a nanofluid inside porous infinite-shaped enclosures suspended by nano-encapsulated phase change materials (NEPCM). Raizah and Aly [23] simulated the double-diffusive convection flow inside a central circular cylinder mounted with two rectangular shapes. The recent research focused on the magnetic field impacts on nanofluid flow within a finned cavity containing solid particles can be found in Ref. [24].

Although the moisture and heat transfer behaviors of porous media have been proposed in several studies [6–24]. However, there are still very few studies that focus on modeling simultaneous heat and moisture transfer during hot water infiltration in partially saturated porous materials. Especially the study considering the influence of infiltration process parameters on transport phenomena with capturing moisture transport in the porous materials has still not been investigated systematically. Therefore, the thermal and moisture dynamic responses of porous media subjected to hot water infiltration have not yet been investigated completely due to the complication correlated with unsaturated transient flow conditions.

The purpose of this paper was to clarify in detail on transport phenomena of hot water infiltration into a two-dimensional granular packed bed. This work was substantially extended from our previous work [20], by incorporating two-dimensional (2D) computational simulation methodology into the calculation of flow and heat transfer during infiltration of hot water. Moreover, we further formulated the complete set of the mathematical model that represents a two-dimensional unsaturated flow and heat transfer during hot water infiltration. A numerical procedure was developed to determine the key characteristics of heat transfer and water infiltration by hot water into the two-dimensional model. The results of the numerical model were validated with the results from previous research. The influences of the water flux supplied and particle size on the water saturation and temperature in the two-dimensional model were investigated systematically. The findings of this study can be used as a basis for further research in this area.

2. Methods and models

This study mainly investigated the transport phenomena of hot water infiltration in a two-dimensional granular packed bed. The first step to understand the thermal and moisture dynamic responses of porous media subjected to hot water infiltration was to calculate the water saturation and its spatial distribution in the packed bed. Thereafter, the convected thermal energy was then transferred to the underside of the packed bed. The complete formulation of the mathematical model represents a two-dimensional unsaturated flow and heat transfer during hot water infiltration was proposed. The numerical scheme based on the control volume

approach was utilized to achieve the solutions of the time-dependent heat and mass transport equations.

2.1. Physical model

A two-dimensional rectangular model was applied to investigate the characteristics of heat transfer and water infiltration by hot water into a two-dimensional granular packed bed. Fig. 1 represents the domain and coordinates information, in which the infiltration of hot water occurred. This model also represents the transport problem in biomedical applications, such as needle-free drug delivery systems, percutaneous infiltration, noninvasive ultrasonic facial rejuvenation system. In this study, the symmetrical model represented the heat transfer and water infiltration within the two-dimensional granular packed bed was utilized to reduce the calculation time while achieving similar accuracy. The granular packed bed model used in this study was considered a dry packing of particles that are being infiltrated by the hot water. The packed bed used can be divided into the void (gas phase) and particles (solid phase). The packed bed model was a rectangular container with 15 cm width (x) and 20 cm height (z). The appropriate domain size selected was directly obtained from a preliminary experiment based on the optimal-size representation of physical phenomena. The particles were homogeneous spheres and thermally isotropic with constant thermal properties.

2.2. Assumptions

The present study emphasized examining the unsaturated flow in this two-dimensional granular packed bed in terms of the influence of the hot water which was supplied. The uniform supply of hot water on the upper surface of the model. The initial composition within the packed bed comprises glass beads and void. A two-phase flow pattern was created around the infiltration front inside the model. It was possible to determine the model which establishes mass and energy for any specific phase by considering conservation equations within the model, by employing a method based on volume averaging [25,26]. Water infiltration occurred when hot water was supplied to the granular packed bed through transfer mechanisms which include gravity and the capillary pressure gradient.

To address the problem, the following assumptions were made:

- 1) The two-dimensional model exhibited rigidity.
- 2) No chemical reaction occurred inside the model.
- 3) The local thermodynamic equilibrium was assumed.
- 4) The flow of liquid and gas was described by Darcy's law.
- 5) The gravity current was considered in performing the flow analysis.
- 6) Gas pressure gradient inside the two-dimensional granular packed bed was neglected.

2.3. Equations for momentum and mass conservation

The microscopic conservation of mass equation for liquid phase is given as shown below [25,26]:

Liquid phase

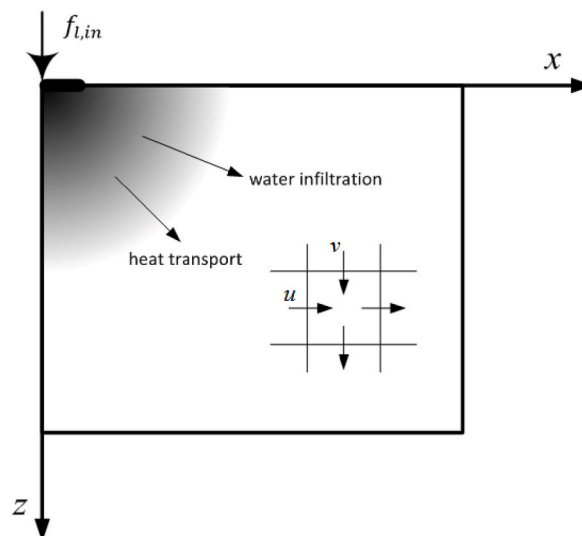


Fig. 1. A symmetrical model represents the heat transfer and water infiltration within the two-dimensional granular packed bed.

$$\varepsilon \frac{\partial}{\partial t} [\rho_l s] = \frac{\partial}{\partial z} \left[\frac{KK_{rl}}{\nu_l} \left(\frac{\partial p_g}{\partial z} - \frac{\partial p_c}{\partial z} - \rho_l g \right) \right] + \frac{\partial}{\partial x} \left[\frac{KK_{rl}}{u_l} \left(\frac{\partial p_g}{\partial x} - \frac{\partial p_c}{\partial x} \right) \right] \quad (1)$$

According to assumption (6); Eq. (1) can be expressed as follows:

$$\varepsilon \frac{\partial}{\partial t} [\rho_l s] = \frac{\partial}{\partial z} \left[\frac{KK_{rl}}{\nu_l} \left(\frac{\partial p_c}{\partial z} - \rho_l g \right) \right] + \frac{\partial}{\partial x} \left[\frac{KK_{rl}}{u_l} \left(\frac{\partial p_c}{\partial x} \right) \right] \quad (2)$$

where ρ is density, s is water saturation, K denotes permeability, K_r indicates the relative permeability, p represents pressure, g is gravitational acceleration, v is velocity in z -direction, u is velocity in x -direction.

2.4. Equations for energy conservation

The energy equation was also modified to be valid in both solid and liquid phases under an assumption of the prevalence of the local thermodynamic equilibrium. It is possible to ignore the kinetic energy and pressure terms since they were not deemed to be important. The temperature distribution of the two-dimensional granular packed can be determined using the energy equation.

$$\frac{\partial}{\partial t} [(\rho_l c_{pl})_T T] + \frac{\partial}{\partial z} [(\rho_l c_{pl} v_l) T] + \frac{\partial}{\partial z} [(\rho_l c_{pl} v_l) T] = \frac{\partial}{\partial z} \left[\lambda_{eff} \frac{\partial T}{\partial z} \right] + \frac{\partial}{\partial x} \left[\lambda_{eff} \frac{\partial T}{\partial x} \right] \quad (3)$$

where $(\rho c)_T$ represents the effective heat capacitance in the porous media, λ_{eff} denotes the effective level of thermal conductivity which is dependent on the extent of water saturation. In conditions of thermal equilibrium, it was possible to calculate the effective heat capacitance by employing the volume average method shown below:

$$(\rho c_{pl})_T = \rho_l c_{pl} \varepsilon s + \rho_p c_{pp} (1 - \varepsilon) \quad (4)$$

where ε is porosity.

Considering the experimental results [18,19] employing glass beads that were fully saturated in water, it was possible to present effective thermal conductivity in terms of the level of water saturation:

$$\lambda_{eff} = \frac{0.8}{1 + 3.78e^{-5.95s}} \quad (5)$$

2.5. Equilibrium relations

In the case of the system of conservation equations which can be derived when considering the multiphase transfer mode, it is necessary to use the constitutive equation involving capillary pressure, p_c , relative permeability K_r , as well as capillary pressure functions, also known as Leverett functions, J . The equation below provides the typical constitutive relationship set for gas and liquid systems:

$$K_{rl} = s_e^3, \quad K_{rg} = (1 - s_e)^3 \quad (6)$$

in which s_e denotes an effective water saturation level described as the irreducible water saturation level, s_{ir} , which has the definition given as [20]:

$$s_e = \frac{s - s_{ir}}{1 - s_{ir}} \quad (7)$$

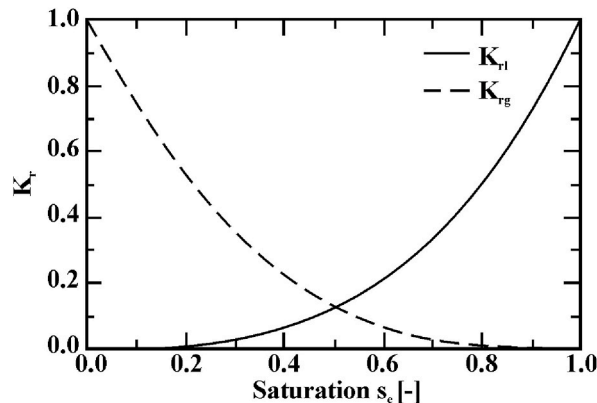


Fig. 2. The relationship between K_r and s_e .

Fig. 2 illustrates the relationships between relative permeability in each of the phases which relate to Eq. (6).

It is assumed that capillary pressure, p_c , is suitably expressed by the well-established Leverett functions, $J(s_e)$. Capillary pressure and water saturation have a relationship that can be described by the application of the Leverett functions, $J(s_e)$ [26].

$$p_c = p_g - p_l = \frac{\sigma}{\sqrt{K/\phi}} J(s_e) \tag{8}$$

where σ is the surface tension, $J(s_e)$ refers to the correlated capillary pressure data provided by Leverett which can be stated as follows:

$$J(s_e) = a(1/s_e - 1)^b \tag{9}$$

In addition, for each condition, the coefficients “a” and “b” are derived from the source [27].

The permeability of the packed bed can be expressed in particle diameter term as [28]:

$$K = \frac{\epsilon^3 d_p^2}{150(1 - \epsilon)^2} \tag{10}$$

where K is permeability (m^2), ϵ is porosity, d_p is particle diameter (m).

2.6. Initial condition and boundary conditions

According to Fig. 1, boundary conditions proposed for the two-dimensional model with the dimensions of 15 cm (x) × 20 cm (z) are shown in Fig. 3 and defined by Eq. (11). It can be supposed that the initial temperature and initial effective water saturation are uniformed at a specific value all over the domain.

$$\begin{aligned} x=0, z=0 & : \rho_l v_l = f_{l, in}, q_{in} = c_{pl} f_{l, in} T_{in} \\ x=0, z \geq 0 & : \rho_l u_l = 0, \frac{\partial T}{\partial x} = 0 \\ x=15, z \geq 0 & : \rho_l u_l = 0, \frac{\partial T}{\partial x} = 0 \\ x \geq 0, z=0 & : \rho_l v_l = 0 \\ x \geq 0, z=20, & \begin{cases} \rho_l v_l = 0 \\ s = 1, q_z = \rho_l c_{pl} v_l T|_{z=20} \end{cases} \end{aligned} \tag{11}$$

The physical properties of the material are given in Table 1.

3. Results and discussion

Numerical simulations of mass, momentum, as well as energy conservation equations, were used to determine the water saturation

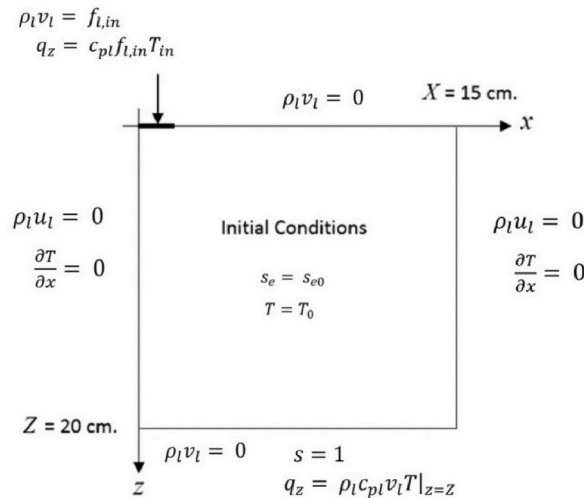


Fig. 3. Initial condition and boundary conditions of a two-dimensional model.

Table 1
Physical properties of the materials [29].

Material properties	Air	Water	Particle
Density, $\rho(\text{kg m}^{-3})$	1.205	1000	2500
Specific heat, $C_p(\text{J kg}^{-1} \text{K}^{-1})$	1007	4186	800
Thermal conductivity, $k(\text{W m}^{-1} \text{K}^{-1})$	0.0256	0.610	1.0
Viscosity, $\mu(\text{kg m}^{-1}\text{s}^{-1}) \times 10^5$	1.9	54.7	-

and temperature distribution in the granular packed beds. The initial temperature of 25 °C was considered to be uniform across the entire model. The supplied water temperature was maintained at 50 °C. The characteristics of heat transfer and hot water infiltration were described in this work. The study employed particles hot of 0.15 mm (fine particles) and 0.40 mm (coarse particles) in diameters. Two porous packed bed systems were investigated, F-Bed (fine particle bed) and C-Bed (coarse particle bed). The influences of two parameters, namely, the particle size (C-Bed and F-Bed) and the fluxes of supplied water ($f = 0.15 \text{ kg/m}^2\text{s}$ and $f = 0.20 \text{ kg/m}^2\text{s}$) have been systematically investigated. We observed the effects associated with each factor and analyze their contributions to water infiltration, water saturation, and temperature.

3.1. Numerical procedure

The water saturation and temperature distributions in the domain subjected to hot water infiltration are calculated using the finite-difference model of the heat and mass transfer model. Since c_p and K_{rg} are dependent on s , the equations for unsaturated flow and heat transfer will be non-linear. The control volume concept was utilized to integrate the generalized system of non-linear equations in the context of typical rectangular control volumes. The solutions of non-linear equations can be obtained using these equations by applying the Newton-Raphson iteration procedure.

3.2. Model verification

In this study, the presented numerical results have been validated against the results which were directly taken from Aoki's work [25]. In the validation, the water was delivered at the packed bed's surface at a constant flux $f = 0.15 \text{ kg/m}^2\text{s}$ with the temperature $T_s = 50 \text{ °C}$. The packed bed contains glass beads having a grain diameter of 0.15 mm. Table 2 shows the comparison between the infiltration front of the present numerical study and that of Aoki. The table illustrates that the infiltration front in the packed bed model of this study and that of Aoki showed an excellent agreement. The agreement from the comparison indicated the accuracy of the proposed numerical model. As a result, the numerical model can be utilized to depict behaviors that occur owing to the water infiltration into a two-dimensional granular packed bed in this study.

3.3. Effect of particle size

The effect of the particle size on the water saturation distribution and heat transport in the two-dimensional granular packed bed was numerically investigated. The result focuses attention on the comparison of F-Bed and C-Bed. Figs. 4 and 5 show the effect of particle size on the transport process in the granular packed beds at the supplied water fluxes of 0.15 $\text{kg/m}^2\text{s}$ and 0.20 $\text{kg/m}^2\text{s}$, respectively. The two-dimensional contour plots in Figs. 4 and 5 are based on the symmetrical plane. The simulated water saturation distributions at various infiltration times are presented in Figs. 4a and 5a. The left half part of each figure represents the F-Bed, and the right half part refers to the C-Bed. The water permeability in the C-bed was relatively high due to a little water retention of large porous particles, causing the water to infiltrate downward quickly and spread only a small distance in the lateral direction. As shown in the results, the water saturation area in the C-bed grew downward faster than the water saturation area in the F-bed. While the F-bed with small particles contained very small continuous pores, had low permeability, and transmitted water very slowly. The water saturation area in the F-bed tended to expand in the lateral direction faster than the downward direction. This was because the capillary pressure of fine particles in the F-bed exerted a significant effect on the water propagation behavior within the packed bed compared to the gravitational force. The high capillary pressure of the F-bed resulted in slowing the infiltration downward and a wider spread of the water distribution over the entire region. In conclusion, the saturation distribution took place because of gravity and capillary backpressure. The capillary pressure gradient governed liquid phase movement, which was also heavily influenced by particle size. For the same supplied water flux, a larger particle size allowed a faster water saturation moving particularly in the gravity direction due to

Table 2
Comparison between infiltration front obtained from the present numerical study and obtained by Aoki et al. [25].

Time (min)	Infiltration front (cm) ($x = 0 \text{ cm}, z$)		% Difference
	Present study	Reference [25]	
10	7.0	7.2	2.78
20	9.9	10.2	2.94
30	12.3	12.5	1.60

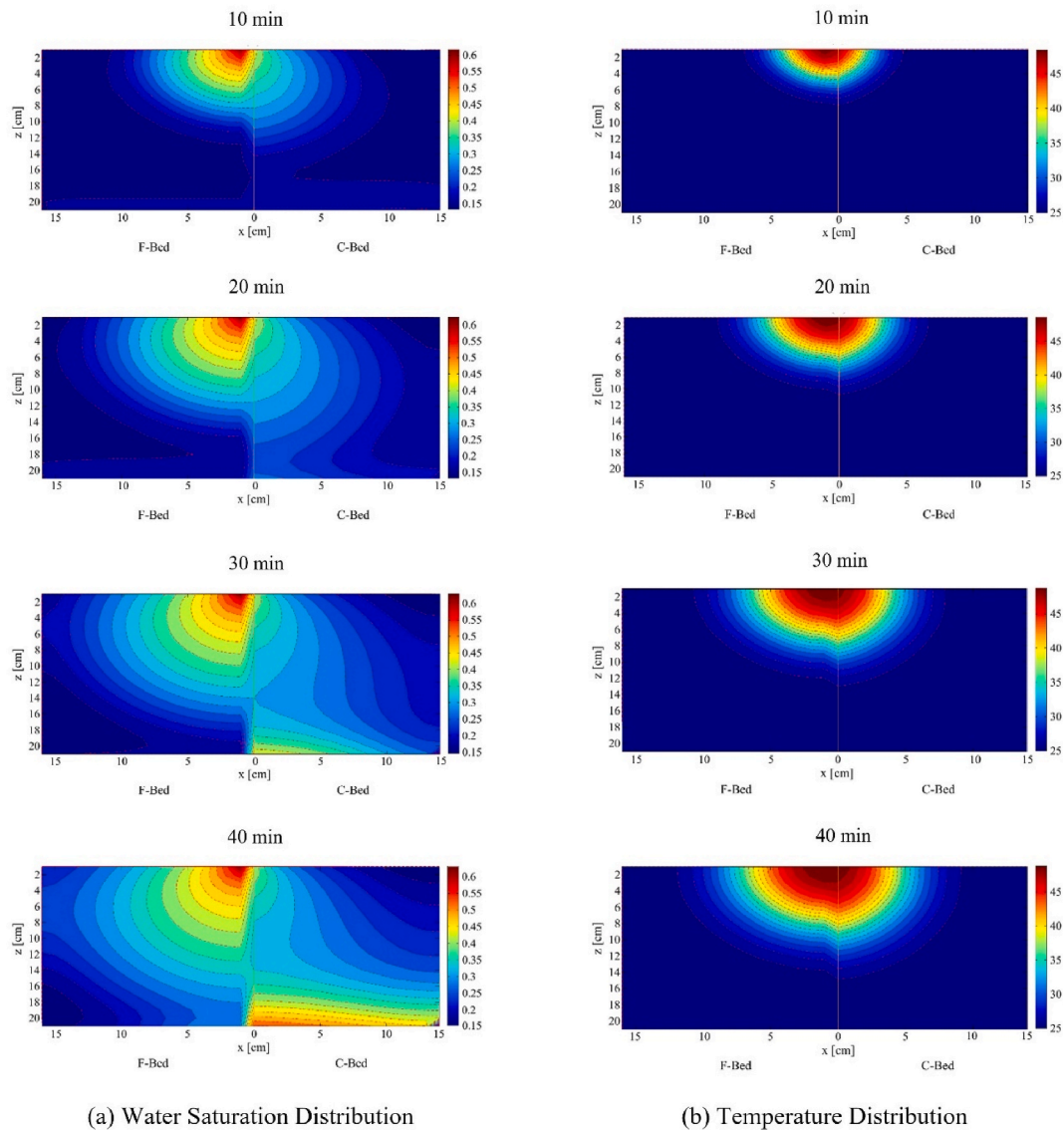


Fig. 4. Comparison of infiltration characteristics in F-bed and C-bed with supplied water flux of $0.15 \text{ kg/m}^2\text{s}$ at various infiltration times: (a) water saturation distribution, (b) temperature distribution.

the gravitational force exerted downward in the z -direction as shown in Figs. 4a and 5a.

Figs. 4b and 5b illustrate the effect of particle size on temperature distribution in the granular packed beds at the supplied water fluxes of $0.15 \text{ kg/m}^2\text{s}$ and $0.20 \text{ kg/m}^2\text{s}$, respectively. The left half part of each figure represents the F-Bed, and the right half part refers to the C-Bed. As seen, the F-bed had a little bit wider heat distribution in x -direction than the C-bed in the upper area, which corresponded to the water saturation spread across the entire area of the F-bed. This was because smaller particles in the F-bed had a large water retention capacity, allowing the water to infiltrate and move slowly. Therefore, the heat had a longer time to be accumulated in the pore space of the small particles on the top layer before it was transmitted down to the bottom layer. Compared to the C-bed on the right side, it has a narrower heat-affected zone, but the heated region penetrates deeper. This is due to the lower water retention capacity and high permeability of the large particle of the C-bed that allows the water to pass through it easily. Besides, it was observed that the heating zone was moving slower than water saturation and a large portion of heat remain undistributed. This was because the high-temperature gradient at the infiltration surface and the long infiltration time led to a drop in temperature in the deep region beneath the infiltration surface.

Fig. 6 shows water saturation and temperature profile of different particle sizes with supplied water flux of $0.20 \text{ kg/m}^2\text{s}$ at infiltration times 15, 30, and 45 min. The water saturation on the vertical axis along the z -direction (at $x = 0$) is illustrated in Fig. 6a. Water infiltration took place from the top to the bottom in the vertical direction because of both gravity and the capillary pressure gradient. In the F-bed ($d = 0.15 \text{ mm}$), the capillary attraction was stronger than the force of gravity, which was tended to allow a limited amount of

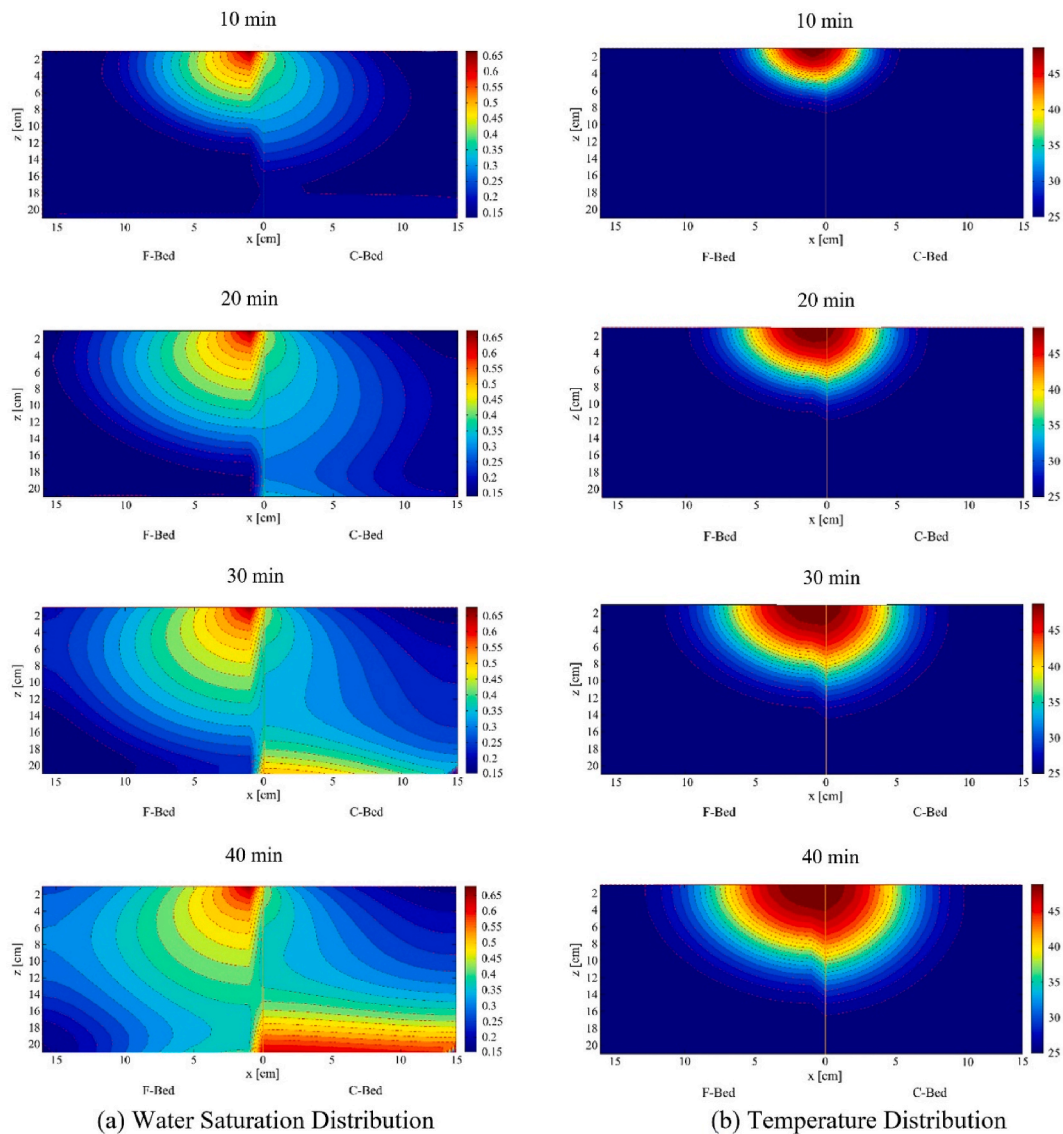
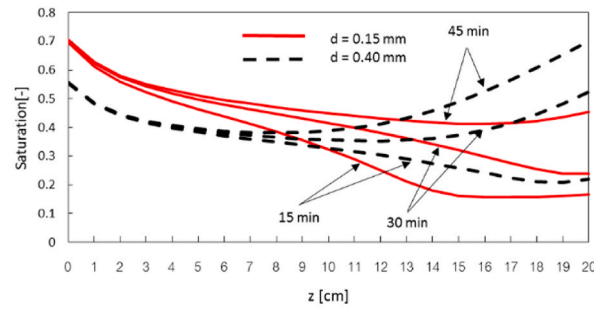


Fig. 5. Comparison of infiltration characteristics in F-bed and C-bed with supplied water flux of $0.20 \text{ kg/m}^2\text{s}$ at various infiltration times: (a) water saturation distribution, (b) temperature distribution.

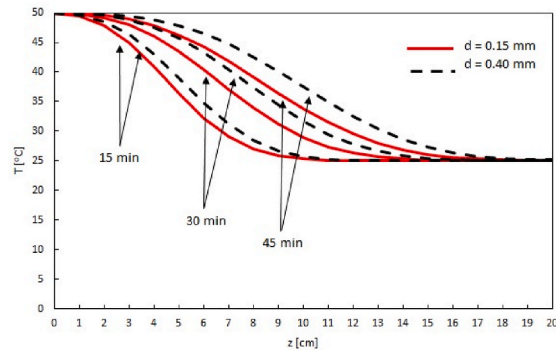
vertical movement of water. The water saturation of the F-bed was, therefore, greater than that of the C-bed in the upper half of the packed bed. While large particles in the C-bed allow the water to move more freely, the inflowing water accumulated in the lower part of the packed bed, establishing the existence of the trapped water at the bottom of the packed bed. The water saturation of the C-bed was, therefore, higher than that of the F-bed in the lower half of the packed bed. Moreover, the increase in time did not significantly affect the water saturation of the F-bed and C-bed around the infiltration surface. Fig. 6b shows temperature on the vertical axis along z -direction (at $x = 0$). The results show that the levels of temperature near the infiltration surface were almost the same as the water temperature at $50 \text{ }^\circ\text{C}$ for both packed beds. This was because the temperature of the packed beds near the infiltration surface was dominated more by the supplied water temperature than the water infiltration effect inside the packed beds. On the other hand, the supplied water temperatures had almost no influence on the temperatures near the bottom of the packed bed. So, the water temperatures in the lower half of both packed beds approach to the room temperature around $25 \text{ }^\circ\text{C}$. However, at any given time, the C-bed achieved significantly higher temperature in any major area of the packed bed by a higher infiltration flow rate that induced the strong convection.

3.4. Effect of supplied water flux

The effect of the supplied water flux on the water saturation distribution and heat transport in the two-dimensional granular packed



(a) Water Saturation



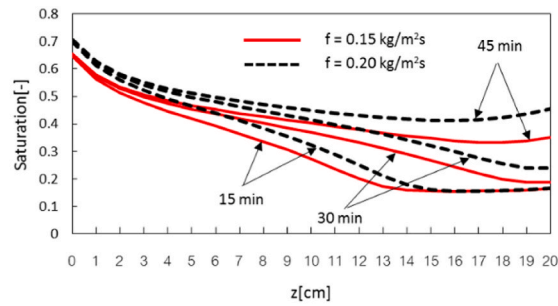
(b) Temperature Profile

Fig. 6. Water saturation and temperature profile of different particle sizes with supplied water flux of $0.20 \text{ kg/m}^2\text{s}$ at various infiltration times: (a) water saturation on the vertical axis (along z -direction at $x = 0$), (b) temperature on the vertical axis (along z -direction at $x = 0$).

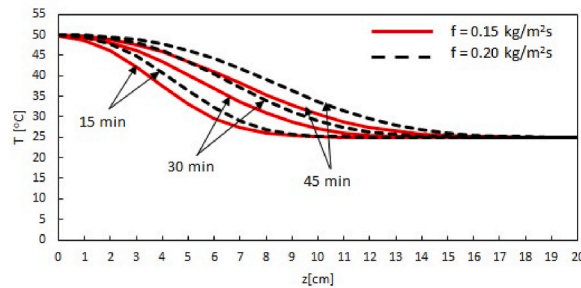
bed was also numerically investigated. The results focused attention on the comparison of two different supplied water fluxes, i.e., 0.15 and $0.20 \text{ kg/m}^2\text{s}$. Figs. 7 shows the effect of supplied water flux on the transport process in the granular packed beds at various infiltration times. Water infiltration took place from the top to the bottom in the vertical direction owing to both gravity and the capillary pressure gradient. The simulated water saturation distributions at various infiltration times are presented in Figs. 7a. For the same particle size, a greater supplied water flux allowed for faster infiltration front moving particularly in the gravity direction due to the gravitational force exerted downward in the z -direction. The higher supplied water flux, the faster infiltration rate and the formation of a higher saturation layer, which was corresponding to the distributions in Fig. 4 ($0.15 \text{ kg/m}^2\text{s}$) and Fig. 5 ($0.20 \text{ kg/m}^2\text{s}$). The higher water saturation also led to the lower capillary back-pressure which was much less than the gravitational effect increasing water infiltration capacity. The water saturation in the packed bed with high supplied water flux was, therefore, greater than that in the packed bed with low supplied water flux. Moreover, the increase in time did not significantly affect the water saturation values in different supplied water fluxes around the infiltration surface. While a higher supplied water flux allowed a faster infiltration rate, so the inflowing water accumulated in the lower part of the packed bed, establishing the existence of the trapped water at the bottom of the packed bed. The water saturation at the bottom of the packed bed was, therefore, higher for a longer period of infiltration time.

Fig. 7b shows temperature on the vertical axis along z -direction (at $x = 0$) of the packed bed at the supplied water fluxes of $0.15 \text{ kg/m}^2\text{s}$ and $0.20 \text{ kg/m}^2\text{s}$. It can be observed that for the same particle size, the temperature presented similar patterns along the z -axis for all cases. When the supplied water flux was larger, the temperature increments propagated deeper and faster in the direction of gravity along the z -direction corresponding to the saturation propagation in Fig. 7a. This was because when increasing the supplied water flux, the gravity effect will overtake the influence of capillary pressure, allowing the infiltration front and heated layer to expand widely in the z -direction. The levels of temperature near the infiltration surface were almost the same with the water temperature at $50 \text{ }^\circ\text{C}$ for both supplied water fluxes. This was because the temperature of the packed beds near the infiltration surface was dominated more by the supplied water temperature than the water infiltration effect inside the packed beds. On the other hand, the supplied water temperatures had almost no influence on the water temperatures near the bottom of the packed bed. So, the water temperatures in the lower half of both packed beds approached the room temperature around $25 \text{ }^\circ\text{C}$. However, at any given time, a higher supplied water flux gave a higher temperature in any major area of the packed bed by a higher infiltration flow rate that induced strong convection.

Fig. 8a and b illustrate the water saturation and temperature respectively at 5 cm depth ($x = 0, z = 5$) against time. The results show



(a) Water Saturation



(b) Temperature Profile

Fig. 7. Water saturation and temperature profile of particle size 0.15 mm (F-bed) with supplied water fluxes of 0.15 and 0.20 kg/m²s at various infiltration times:

- (a) water saturation on the vertical axis (along z -direction at $x = 0$),
 (b) temperature on the vertical axis (along z -direction at $x = 0$).

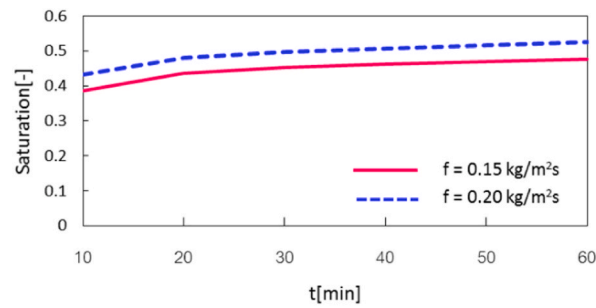
the water saturation and temperature of particle size 0.15 mm (F-bed) with supplied water fluxes of 0.15 and 0.20 kg/m²s as a function of time. As time passes, increased supplied water flux resulted in higher water saturation and temperature. The water saturation and temperature for the supplied water flux of 0.20 kg/m²s were significantly higher than those of 0.15 kg/m²s along the infiltration time. This was due to the greater flow velocity in the higher supplied water flux greatly contributing to increasing infiltration rate and flow convection in the packed bed especially in a high-temperature zone. The findings suggest that the supplied water flux, therefore, plays an important role in water infiltration and heat transfer in the granular packed bed. Thus, it can be inferred from this study that simultaneous heat transfer and water infiltration are significantly governed by internal and external thermal interaction phenomena associated with the hot water infiltration process.

4. Conclusions

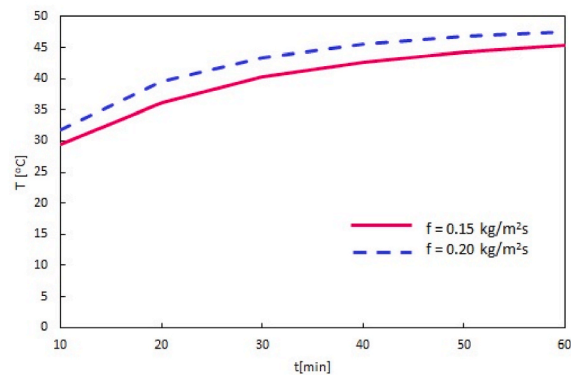
A numerical investigation of the water infiltration and transport phenomena of hot water infiltration in a two-dimensional granular packed bed was performed. In this study, the effects of particle size, and supplied water flux on water saturation and temperature in the porous packed bed were addressed. In addition, we evaluated the influence of hot water on heating-shape and heating location. In the calculation procedure, we further formulated the complete set of the mathematical model that represents a two-dimensional unsaturated flow and heat transfer during hot water infiltration. A numerical procedure was developed to determine the key characteristics of heat transfer and water infiltration by hot water into the two-dimensional granular packed bed. The results of the numerical model were validated with the results from previous research. The influences of the particle size and supplied water flux on the water saturation distribution and heat transport in the two-dimensional granular packed bed were investigated systematically. The key findings can be summarized as follows:

1) The water saturation distribution took place owing to gravity and capillary backpressure. Larger particle size in C-bed allowed a faster water saturation moving especially in the direction of gravity due to the gravitational force exerted downward in the z -direction. The water saturation and heating area in the case of fine particles (F-bed) tended to expand in the lateral direction faster than the downward direction. This was because the capillary pressure of fine particles exerts a significant effect on the water propagation behavior inside the packed bed compared to the gravitational force. The F-bed exhibited a little bit wider heat distribution than the C-bed in the upper area, which corresponded to the water saturation spread across the entire area of the F-bed. At any given time, the C-bed achieved significantly higher temperature in the major area of the packed bed by a higher infiltration flow rate that induced the strong convection.

2) The greater supplied water flux resulted in deeper water saturation. The temperature increments of the higher supplied water



(a) Water Saturation



(b) Temperature

Fig. 8. Water saturation and temperature of particle size 0.15 mm (F-bed) with supplied water fluxes of 0.15 and 0.20 kg/m²s as a function of time: (a) water saturation at 5 cm depth ($x = 0, z = 5$), (b) temperature at 5 cm depth ($x = 0, z = 5$).

flux propagated deeper and faster in the direction of gravity along the z -direction corresponding to the saturation propagation. This was because when increasing the supplied water flux, the gravity effect will overtake the influence of capillary pressure, allowing the infiltration front and heated layer to expand widely in the z -direction. The increase in time did not significantly affect the water saturation values around the infiltration surface in different supplied water fluxes. While the greater supplied water flux allowed the faster infiltration rate, so the inflowing water accumulated in the lower part of the packed bed, establishing the existence of the trapped water at the bottom of the packed bed. The water saturation at the bottom of the packed bed was, therefore, higher for a longer period of infiltration time. Furthermore, the heating area was found to be expanding slower than the water saturation front in all conditions.

A better understanding of the influences that affect the hot water infiltration and transport phenomena in the granular packed bed has been identified. Based on the research findings, it is possible to conclude that the particle size and supplied water flux have a considerable impact on the water saturation and heat transfer of the granular packed bed during exposure to hot water infiltration. The obtained results provide a function for a basic understanding of heat transfer and water infiltration in granular packed beds. The findings can be used as basic information for numerous creative and innovative applications in several fields of engineering and medicine.

CRediT authorship contribution statement

Sauce Aksornkitti: Conceptualization, Validation, Investigation, Writing – original draft, preparation. **Phadungsak Rattana-decho:** Supervision, Funding acquisition, Project administration. **Teerapot Wessapan:** Visualization, Writing – review & editing.

Declaration of competing interest

The authors declare that they have no known competing financial interests or personal relationships that could have appeared to influence the work reported in this paper.

Acknowledgements

This study was supported by Thailand Science Research and Innovation Fundamental Fund (Project No. 66082) and the Program Management Unit for Human Resources & Institutional Development, Research and Innovation, NXPO (grant number B05F630092). The authors are pleased to acknowledge the Thammasat Ph.D. scholarship program for supporting this research work.

Nomenclatures

c_p	specific heat, (J/kg.K)
d_p	particle diameter (m)
g	gravitational acceleration, (m/s ²)
K	permeability, (m ²)
K_r	relative permeability
p	pressure, (pa)
p_c	capillary pressure, (pa)
q	heat flux, (W/m ³)
s	water saturation
t	time, (min)
T	temperature, (°C)
u	velocity in x-axis, (m/s)
v	velocity in z-axis, (m/s)

Greek letters

ε	porosity
ρ	density, (kg/m ³)
λ	effective thermal conductivity, (W/mK)
σ	surface tension, (N/m)
f	supplied water flow rate, (kg/m ² s)

Subscripts

l	liquid phase
g	gas phase

References

- [1] A. Mohizin, D. Lee, J.K. Kim, Impact of the mechanical properties of penetrated media on the injection characteristics of needle-free jet injection, *Exp. Therm. Fluid Sci.* 126 (2021) 110396.
- [2] R.P. Widmer, S.J. Ferguson, A mixed boundary representation to simulate the displacement of a biofluid by a biomaterial in porous media, *J. Bioeng.* 133 (5) (2011), 051007.
- [3] R. Liu, J. Wang, H. Zhan, Z. Chen, W. Li, D. Yang, S. Zheng, Influence of thick karst vadose zone on aquifer recharge in karst formations, *J. Hydro.* 592 (2021) 125791.
- [4] R. Morbidelli, C. Corradini, C. Saltalippi, A. Flammini, J. Dari, R.S. Govindaraju, Rainfall infiltration modeling: a review, *Water* 10 (12) (2018) 1873.
- [5] T. Wessapan, P. Rattanadecho, Acoustic streaming effect on flow and heat transfer in porous tissue during exposure to focused ultrasound, *Case Stud. Therm. Eng.* 21 (2020) 100670.
- [6] C. Hammecker, A.C.D. Antonino, J.L. Maeght, P. Boivin, Experimental and numerical study of water flow in soil under irrigation in northern Senegal: evidence of air entrapment, *Eur. J. Soil Sci.* 54 (3) (2003) 491–503.
- [7] H. Gvirtzman, E. Shalev, O. Dahan, Y.H. Hatzor, Large-scale infiltration experiments into unsaturated stratified loess sediments: monitoring and modeling, *J. Hydro.* 349 (1–2) (2008) 214–229.
- [8] Y. Ma, S. Feng, D. Su, G. Gao, Z. Huo, Modeling water infiltration in a large layered soil column with a modified green-ampt model and HYDRUS-1D, *Comput. Electron. Agric.* 715 (2010) 540–547.
- [9] I.W. Ayu, S. Priyono, Soemarno, Assessment of infiltration rate under different drylands types in unter-iwes subdistrict sumbawa besar, Indonesia, *J. Nat. Sci. Res.* 3 (10) (2013) 71–77.
- [10] P. Langston, A.R. Kennedy, Discrete element modelling of the packing of spheres and its application to the structure of porous metals made by infiltration of packed beds of NaCl beads, *Powder Technol.* 268 (2014) 210–218.
- [11] Y. Xiong, Flow of water in porous media with saturation overshoot: a review, *J. Hydro.* 510 (2014) 353–362.
- [12] E.J. Henry, J.E. Smith, Numerical demonstration of surfactant concentration-dependent capillarity and viscosity effects on infiltration from a constant flux line source, *J. Hydro.* 329 (1–2) (2006) 63–74.
- [13] N. Romano, B. Brunone, A. Santini, Numerical analysis of one-dimensional unsaturated flow in layered soils, *Adv. Water Resour.* 21 (4) (1998) 315–324.
- [14] C. Corradini, F. Melone, R.E. Smith, Modeling local infiltration for a two-layered soil under complex rainfall patterns, *J. Hydro.* 237 (2000) 58–73.
- [15] H. Gomez, L. Cueto-Felgueroso, R. Juanes, Three-dimensional simulation of unstable gravity-driven infiltration of water into a porous medium, *J. Comput. Phys.* 238 (2013) 217–239.
- [16] B. Sayah, M. Gil-Rodriguez, L. Juana, Development of one-dimensional solutions for water infiltration: analysis and parameters estimation, *J. Hydro.* 535 (2016) 226–234.
- [17] T. Bandai, S. Hamamoto, G.C. Rau, T. Komatsu, T. Nishimura, The effect of particle size on thermal and solute dispersion in saturated porous media, *Int. J. Therm. Sci.* 122 (2017) 74–84.
- [18] N. Moussa, D. Gobin, H. Duval, B. Goyeau, Infiltration of a porous matrix by a solidifying liquid metal: a local model, *Int. J. Therm. Sci.* 120 (2017) 481–490.

- [19] S. Suttisong, P. Rattanadecho, The experimental investigation of heat transport and water infiltration in granular packed bed due to supplied hot water from the top: influence of supplied water flux, particle sizes and supplied water temperature, *Exp. Therm. Fluid Sci.* 35 (2011) 1530–1534.
- [20] P. Rattanadecho, S. Suttisong, T. Somtawin, The numerical and experimental analysis of heat transport and water infiltration in a granular packed bed due to supplied hot water, *Numer. Heat Tran, Appl.* 65 (2014) 1007–1022.
- [21] A.M. Aly, E.M. Mohamed, N. Alsedais, ISPH analysis of thermosolutal convection from an embedded I-Shaped inside an inclined infinite-shaped enclosure suspended by NEPCM, *Case Stud. Therm. Eng.* 26 (2021) 101071.
- [22] A.M. Aly, E.M. Mohamed, M.F. El-Amin, N. Alsedais, Double-diffusive convection between two different phases in a porous infinite-shaped enclosure suspended by nano encapsulated phase change materials, *Case Stud. Therm. Eng.* 26 (2021) 101016.
- [23] Z. Raizah, A.M. Aly, Double-diffusive convection of a rotating circular cylinder in a porous cavity suspended by nano-encapsulated phase change materials, *Case Stud. Therm. Eng.* 24 (2021) 100864.
- [24] A.M. Aly, E.M. Mohamed, N. Alsedais, The magnetic field on a nanofluid flow within a finned cavity containing solid particles, *Case Stud. Therm. Eng.* 25 (2021) 100945.
- [25] K. Aoki, M. Hattori, M. Kitamura, N. Shiraishi, Characteristics of Heat Transport in Porous Media with Water Infiltration, *ASME JSME Therm. Eng. Joint Confer, United States*, 1991.
- [26] P. Rattanadecho, K. Aoki, M. Akahori, Influence of irradiation time, particle sizes, and initial moisture content during microwave drying of multi-layered capillary porous materials, *J. Heat Tran.* 124 (2002) 151–161.
- [27] P. Rattanadecho, K. Aoki, M. Akahori, Experimental and numerical study of microwave drying in unsaturated porous material, *Int. Commun. Heat Mass Tran.* 28 (5) (2001) 605–616.
- [28] A. Amiri, K. Vafai, Analysis of dispersion effects and non-thermal equilibrium, non-Darcian, variable porosity incompressible flow through porous media, *Int. J. Heat Mass Tran.* 37 (1994) 939–954.
- [29] N. Suwannapum, P. Rattanadecho, Analysis of heat–mass transport and pressure buildup induced inside unsaturated porous media subjected to microwave energy using a single (TE₁₀) mode cavity, *Dry. Technol.* 29 (2011) 1010–1024.